1	Carbon and nitrogen productivity during spring in the oligotrophic Indian Ocean along the
2	GO-SHIP IO9N transect
3	
4	Steven E. Baer ^{a,*,#} , Sara Rauschenberg ^a , Catherine A. Garcia ^b , Nathan S. Garcia ^b , Adam C.
5	Martiny ^{b,c} , Benjamin S. Twining ^a , Michael W. Lomas ^a
6	
6	
7	^a Bigelow Laboratory for Ocean Sciences, 60 Bigelow Drive, East Boothbay, Maine 04543 USA
8	^b Department of Earth System Science, University of California, 3208 Croul Hall, Irvine,
9	California 92697 USA
10	^c Department of Ecology and Evolutionary Biology, University of California, 321 Steinhaus
11	Hall, Irvine, California 92697 USA
12	#current address: Corning School of Ocean Studies, Maine Maritime Academy, Castine, Maine
13	04421
14	
15	
16	*correspondence: sbaer@bigelow.org
17	
18	
19	
20	
21	
22	

23 Highlights:

- Surface plankton assemblage dominated by smallest plankton: heterotrophic bacteria and the autotrophic single-celled cyanobacteria, *Prochlorococcus*.
 - Generally low absolute uptake rates of C and N due to low biomass, but specific rates suggest an actively growing community.
 - Primary production and nitrogen uptake rates reach local maxima around 5°N. The fratio does not show a local maxima, and mean values over the whole transect are considerably higher than other oligotrophic regions of the global ocean.
 - Dissolved organic compounds are the dominant biogeochemical currency in this region, with urea having the highest uptake rates of N species tested, dissolved organic phosphorus found at high concentrations, and a potentially local source of dissolved organic carbon.

Abstract

There is limited biogeochemical rate data from the oligotrophic central Indian Ocean, but it is known that there are geographical gradients in the physical and chemical conditions that may lead to unique biogeochemical regimes. As participants on a GO-SHIP repeat hydrography cruise, a transect was completed in spring of 2016 from 28°S to 18°N in the Indian Ocean, roughly along the 95°E meridion. Cell count samples (phytoplankton and heterotrophic bacteria) analyzed by flow cytometry, and samples for carbon and nitrogen productivity incubations, assessed by stable isotopic tracers, were obtained from 20 m at approximately every other degree of latitude. Microbial cell counts by flow cytometry indicate that *Prochlorococcus* was the principal autotroph, but with increasing contributions of *Synechococcus* around the equator.

46 Large eukaryotes (>20 µm), imaged using FlowCAM, were generally absent or in very low 47 abundance (<0.5 µg C L⁻¹) from near-surface waters. Heterotrophic bacteria contributed 28.4 ± 48 4.6% of the microbial community biomass and were positively correlated to autotrophic biomass. 49 Dissolved nitrate and phosphate concentrations were below detection limits throughout the 50 surface 50 m, while ammonium was undetectable at almost all stations and depths. In the 50-200 51 m depth range, nitrate and phosphate concentrations steadily increased from south to north, 52 reaching a maximum of 31 and 2.2 µM respectively north of 6°N. The ratio of dissolved NO₃ :PO₄ standing stocks was always below 15. Urea concentrations (0.02-0.18 µmol L⁻¹) showed 53 54 an increasing trend towards the north and dissolved organic phosphorus concentrations (0.25-0.37 µmol L⁻¹) had a maxima between 5-15°S. Absolute uptake rates of nitrate, ammonium and 55 urea were all less than 1.5 nmol N L⁻¹ h⁻¹ south of 15°S, and increased until local maxima of 3.4, 56 9.0, and 21 nmol N L⁻¹ h⁻¹ for nitrate, ammonium, and urea respectively, were reached between 57 58 1.5-6.5°N. Ammonium and urea uptake rates were consistently 3-8 times higher than nitrate 59 uptake rates, with a mean f-ratio of 0.23 for the entire transect. Primary production followed the same trend of nitrogen uptake, with a local maximum of 7.4-10.8 nmol C L⁻¹ h⁻¹ found 1.5-6.5°N. 60 61 These data represent some of the first reported measurements of primary production, nitrogen 62 uptake, and phytoplankton diversity across biogeochemical provinces in the central oligotrophic 63 Indian Ocean a large but understudied region of the global ocean.

64

65

66

Keywords

Indian Ocean, primary production, *Prochlorococcus*, nitrogen uptake, DOM

68

1 Introduction

69

70

71

72

73

74

75

76

77

78

79

80

81

82

83

84

85

86

87

88

89

90

91

The Indian Ocean (IO) accounts for 15-20% of global ocean net primary production (Behrenfeld and Falkowski, 1997) and the northern regions (Arabian Sea and Bay of Bengal) contain major oxygen minimum zones with extensive nitrogen (N) loss (Naqvi et al., 2000; Ward et al., 2009). While the IO is likely a key component in global ocean biogeochemical cycles, we currently have a limited understanding of the variation in and control on phytoplankton diversity and productivity in the oligotrophic IO and the linkages between marine biota and biogeochemical functioning. There has been extensive work done on the biogeochemistry of the northern, eastern, and southern IO, including the Arabian Sea (e.g. Garrison et al., 2000; Morrison et al., 1998; Owens et al., 1993), the Bay of Bengal (e.g. Kumar et al., 2004; Madhupratap et al., 2003), the Leeuwin Current around Australia (see Waite et al., 2007 and references therein), and the Indian section of the Southern Ocean (e.g. Bianchi et al., 1997; Schlüter et al., 2011; Thomalla et al., 2011). These regions in the broad perimeter of the IO tend to have relatively high nutrient inputs, biomass, and large size classes of phytoplankton, but are separated from the central oligotrophic IO by large frontal systems or simply distance. Most of the data from the open ocean region of the IO derives from the International Indian Ocean Expedition (IIOE) in the 1960's, several WOCE repeat lines, and a few individual cruises (Bouman et al., 2006; Fernandes et al., 2008; Martiny et al., 2009; Prakash et al., 2015; Sorokin et al., 1985). However, these studies had a limited geographic range, focused primarily on inorganic nutrient measurements and hydrography, and offered a limited characterization of phytoplankton biodiversity, productivity, and N uptake (Brewin et al., 2012; Hood et al., 2009; Wiggert et al., 2006). Satellite-based models of chlorophyll and net primary production indicate a potential decrease in biomass and productivity over the past few decades (Behrenfeld et al.,

2006; Roxy et al., 2016), however other models have isolated the central IO as one of the only regions in the world to have increasing chlorophyll (Boyce et al., 2010). There are few field-based measurements of chlorophyll, carbon, and productivity in this area of the central oligotrophic IO.

92

93

94

95

96

97

98

99

100

101

102

103

104

105

106

107

108

109

110

111

112

113

Despite our limited knowledge of oligotrophic IO biological dynamics, physical and chemical conditions have been well described. The physico-chemical environments vary latitudinally, which may lead to unique biological and biogeochemical regimes. The Indian Southern Subtropical Gyre (ISSG, approximately 10-30°S) likely has very low dissolved N:P ratios (~4) in the photic zone, with relatively low diffusive nutrient input fluxes. This may in part be due to N loss and the outcome is a N stressed region. The region may further be co-stressed by iron – although there is considerable uncertainty in the estimate of dust deposition in this region (Grand et al., 2015; Mahowald et al., 2005). Limited iron availability may restrict N fixation and therefore enhance N stress. This may lead to the ultraoligotrophic nature of the ISSG and likely leads to unique community composition and functioning, both in terms of the abundance of specific lineages and their physiology (e.g., high affinity to nutrients in short supply). The central IO (~0-10°S) has elevated dissolved nutrient diffusive input fluxes due to upwelling, and high dissolved N:P ratios but low dissolved iron concentrations (Grand et al., 2015; Thi Dieu Vu and Sohrin, 2013; Wiggert et al., 2006). The InterMonsoon Gyre (IMG) in the north has elevated concentrations of reduced N compounds due to riverine inputs, but overall significant N loss due to denitrification associated with the oxygen minimum zone in the Bay of Bengal (Hood et al., 2009). High rates of "new" production in Bay of Bengal support high carbon (C) export and contribute to the oxygen minimum zone (Kumar et al., 2004). The

northern IO region is also characterized by sea-surface temperatures >30°C, and appears to be warming faster than most other ocean basins (Alory and Meyers, 2009).

As part of the Global Ocean Ship-Based Hydrographic Investigations Program (GO-SHIP), we sampled a transect in the oligotrophic central IO roughly along the 95°E meridian (Figure 1). The GO-SHIP program constitutes repeat hydrography transects throughout the global ocean, focused on a standard suite of mostly physical (e.g. temperature, salinity, oxygen saturation) and chemical (e.g. nutrient concentrations) parameters. Our goal for this study was to capture a snapshot of the planktonic community composition, along with estimates of their carbon productivity and nitrogen uptake rates. Additional measurements were made to quantify the organic compounds urea and dissolved organic phosphorus (DOP). The biological community was assessed by measuring chlorophyll a (chl a) concentrations along with flow cytometry analysis of heterotrophic bacteria and autotrophic cells from 0.2 – 200 um. Literature values were used to calculate taxon-specific biomass of single-cell cyanobacteria, nanoeukaryotes, and large phytoplankton (>20 µm). Incubations for uptake rate calculations were performed with ¹³C and multiple ¹⁵N (nitrate, ammonium, urea) tracers. This work provides a seasonal snapshot of the diversity and productivity throughout a broad range of the oligotrophic central basin of the IO. Detailed information on the microbial community and their activity across the three proposed biogeochemical provinces (ISSG, CIO, and IMG) will improve the datasets for groundtruthing remote sensing and production algorithms.

133

114

115

116

117

118

119

120

121

122

123

124

125

126

127

128

129

130

131

132

134

135

2 Materials and methods

2.1 Sampling

The GO-SHIP cruise travelled from Perth, Australia to Phuket Thailand primarily along 95°E from March 21, 2016 - April 28, 2016. This sampling regime was designed to cover a large geographic area, but at one degree of latitude coverage, we were not able to resolve any mesoscale structures (e.g. eddies). Temperature and salinity data were collected from CTD (SeaBird Electronics) downcasts. Temperature and conductivity sensors were calibrated before and after the cruise, and duplicate sensors were cross-referenced for precision. Discrete depth samples were collected from 10 L Niskin bottles mounted on a rosette. Inorganic nutrients (dissolved inorganic carbon, nitrate, and phosphate) were sampled using clean technique and run onboard using standard methods (below). The full GO-SHIP program data set for this cruise can be found at https://cchdo.ucsd.edu/cruise/33RR20160321. At a subset of stations (see Table 1 and Figure 1 for specific locations), samples that are not part of the standard GO-SHIP program were collected for chl *a*, urea, DOP, flow cytometry, and incubations for nutrient uptake as described below. Uptake experiments were performed once per day, and targeted the CTD cast encompassing solar noon during the six-hour incubation period.

2.2 Physics

The mixed layer depth was determined to be the first depth at which the difference in density from the surface was 0.03 kg m⁻³ (Weller and Plueddemann, 1996). The nutricline was determined to be the first depth where nitrate was greater than 0.05 µmol N L⁻¹ (Cermeño et al., 2008).

Because macronutrient concentrations were below detection limits (<0.05 μmol N or P L⁻¹) in the surface, we calculated flux rates through the nutricline to better understand nutrient inputs and availability. The flux rates were calculated as the gradient in concentration (μmol m⁻¹) across the nutricline multiplied by the vertical diffusivity coefficient (K_z; m² s⁻¹). CTD-chipod data obtained during the cruise at three process stations (97, 127, and 162) were used to determine Kz for each of the three defined regions. The mean of three 10 m bin values centered on the nutricline depth for each region were used. K_z values were 2.5x10⁻⁵, 3.3x10⁻⁵, and 5.0x10⁻⁵ m² s⁻¹ for the ISSG, CIO, and Bay of Bengal respectively (J. Nash, pers. comm.).

2.3 Nutrients

Nutrient analyses were run onboard by the Oceanographic Data Facility, with methods described in the nutrient section of the GO-SHIP repeat hydrography manual (Hydes et al., 2010). Briefly, nitrate, nitrite, and phosphate were run on a Seal Analytical continuous-flow AutoAnalyzer 3. Primary standards were made each day and used to calibrate the instrument. Detection limits were $0.05~\mu mol~L^{-1}$. Samples for urea and total dissolved phosphorus (TDP) were collected into 60 mL amber high-density polyethylene bottles after filtration through GF/F filters (nominal pore size = $0.7~\mu m$). Bottles were kept frozen at -80°C until analysis in the lab, within 6 months of collection. Urea analysis was run in duplicate using the room-temperature monoxime method (Goeyens et al., 1998; Price and Harrison, 1987); detection limit of this analysis was $0.01~\mu mol~N~L^{-1}$. TDP concentrations were quantified by acid persulfate oxidation (Ridal and Moore, 1990) as modified by Lomas et al. (2010). Detection limits for TDP are $0.008~\mu mol~L^{-1}$. Dissolved organic phosphorus (DOP) concentrations were determined as TDP minus phosphate; where phosphate values were higher than TDP, DOP was assumed to be zero.

2.4 Phytoplankton

180

181

182

183

184

185

186

187

188

189

190

191

192

193

194

195

196

197

198

199

200

201

202

Chl a was a combination of live samples analyzed onboard by the lab of N. Nelson, and frozen samples analyzed within 2 months in the laboratory. Both live and frozen samples were collected on GF/F filters and analyzed with acetone extraction on a calibrated Turner AU-10 fluorometer (Parsons et al., 1984). Data presented in this manuscript are a combination of the live and frozen data sets. Flow cytometry samples were collected directly from the Niskin bottle into 2 ml cryovials and fixed with a freshly made and 0.2 µm-filtered 10% paraformaldehyde solution, at a final concentration of 0.5% (v/v). Samples were allowed to fix for 1 hour in the dark at 4-5°C, and then kept at -80°C until analysis. Counts were performed on a BD FacsJazz flow cytometer equipped with a 200 mW 488 nm laser, with filters for 530, 580 and 690 nm. Daily instrument calibrations were performed with 3 µm 6-peak beads (Spherotech) and the forward scatter signal normalized with 0.53 µm beads (e.g. Casey et al., 2013). Prochlorococcus was identified by forward scatter and red fluorescence, and *Synechococcus* distinguished by emission in the orange wavelengths. Small eukaryotes were identified as the autofluorescing cells outside of the cyanobacterial (i.e. *Prochlorococcus* and *Synechococcus*) gates. Biomass estimates were based on the relationship between normalized forward scatter and C per cell described in Casey et al. (2013). Bacterial counts were determined after 10 minutes of staining with SYBR Green (Marie et al., 1997), and biomass was estimated assuming 12 fg C cell⁻¹ (Fukuda et al., 1998). Larger cells (>20 µm) were enumerated on live pre-concentrated samples using a FlowCAM (Fluid Imaging Technologies, Scarborough Maine). Approximately 8 L of seawater was reverse concentrated through a 10 μm mesh, and then rinsed with 0.2 μm filtered seawater;

final volumes were between 50 and 100 mL per station and depth. Samples were analyzed using

a 200 µm flow cell and a 4X objective, with cell fluorescence triggered by a 50 mW 488 nm laser. Only cells larger than 20 µm were counted, and biomass was estimated from genus-level identification and biovolume-to-carbon conversions from the literature (Menden-Deuer and Lessard, 2000; Sieracki et al., 1989).

2.5 Incubations

203

204

205

206

207

208

209

210

211

212

213

214

215

216

217

218

219

220

221

222

223

224

225

Uptake experiments were performed in duplicate 2 L polycarbonate bottles. Additions of ¹³C-bicarbonate (99% ¹³C: Cambridge Isotope Laboratories) were made at a final concentration of 205 µmol C L⁻¹, which corresponded to a mean and standard deviation atom percent enrichment of 10.4 ± 0.2 (n = 144). N additions of ¹⁵N-nitrate, -ammonium, and -urea were made at a final concentration of 0.03 µmol N L⁻¹. The values of the N species were expected to be below method detection limits (0.05 µmol N L⁻¹), we chose this concentration to be as low as reasonable and still expect to discern a signal. Atom percent enrichment for nitrate and ammonium were a mean and standard deviation 54 ± 0.3 , while urea had an atom percent enrichment of 38 ± 15 (n = 48 for each substrate). Bottles were placed in an incubator on deck equipped with a surface flow-through system. Temperature in the incubation bottles was monitored in an additional 2 L bottle containing a HOBO temperature logger (Onset Computer Corporation). After a 6-hour incubation, samples were filtered via peristaltic pump over precombusted (450°C for 4 h) GF/F filters contained in plastic twist-lock housings. Filters were stored in sterile cryovials and frozen at -80°C until analysis. The filtration system was rinsed with 10% HCl and then flushed with Milli-Q water after every use. Mass and isotope enrichment measurements were performed by Bigelow Analytical Services, utilizing a Thermo Finnigan Delta V mass spectrometer. Uptake rates were calculated for N as per Dugdale and Goering (1967) and for C as per Hama et al. (1983). Particulate organic C and N were assumed

to have an atom percent normal of the global average (1.071 and 0.3986 for C and N respectively). Where dissolved N concentrations were below detection limit, ambient concentrations were assumed to be half of the detection limit (0.025, 0.025, and 0.005 µmol N L for nitrate, ammonium, and urea respectively). Dissolved inorganic carbon measurements, determined by Single Operator Multi-parameter Metabolic Analyzer (Dickson et al., 2007), were used for ambient C concentrations in the rate calculations.

Phytoplankton growth rates were calculated from carbon productivities. The carbon uptake rate was divided by the total phytoplankton biomass, and then adjusted for decomposition rates and daily PAR during the incubations. The mean value $(34.2 \pm 3.3\%)$ for open ocean phytoplankton (Duarte and Cebrián, 1996) was used for decomposition rates. Daylight hours were adjusted by calculating the percentage of PAR during the incubation compared to the total daily PAR experienced at that station. Daily PAR values were obtained from the Rolling Deck Repository Program (https://doi.org/10.7284/121708), and PAR in the incubation bottles was monitored by a HOBO data logger.

2.6 Statistics

Statistical comparisons within and between regions were conducted using SigmaPlot (Systat Software; version 12.0). For comparisons of mean values among regions, Student's t-tests were conducted, and for parameter trends between regions Spearman rank order correlations were performed. Significance for both tests was assessed at p <0.05.

3 Results

249

250

251

252

253

254

255

256

257

258

259

260

261

262

263

264

265

266

267

268

269

270

271

3.1 Physics and chemistry

In the ISSG, temperatures in the surface 20 m increased from 22 to 29°C going from 28°S to 10°S. Between 10°S and 14°N, temperatures in the surface 20 m were consistently 30 to 31°C, and only slightly cooler in the Bay of Bengal, at an average of 30°C (Figure 2). Salinity ranged from 34.4 to 35.1 throughout the ISSG and CIO. In the IMG, north of 6°N and into the Bay of Bengal salinity values in the surface 50 m were lower, with a range of 32.1 to 33.5, likely due to the freshwater inputs (Sengupta et al., 2006). The ISSG was well-mixed down to a relatively deep (~130m) nutricline (Figure 3). Both the mixed layer depth and the nutricline depth were relatively stable throughout the CIO and IMG, with a mean and standard deviation of 20.7 ± 11.3 and 60.3 ± 13.9 respectively. The minimum difference in depth (<19 m) between the mixed layer (MLD) and nutricline was found in the CIO between 5.0-7.0°N. In a broad sense, the ISSG was distinguished by its relatively high salinity water and deep mixed layer. The CIO and IMG had a sharp gradient in temperature at approximately 50 m depth. During the transit, no eddies could be resolved due to the relatively low spatial resolution of the CTD casts. Calculated diffusive fluxes for both nitrate and phosphate were low (<0.4 and 0.03 µmol m⁻² d⁻¹ respectively) and stable in the southern ISSG from 28°S to 17°S (Figure 3). Both fluxes increased linearly ($R^2 = 0.75$ and 0.81 for nitrate and phosphate respectively) moving north from 17°S for the remainder of the transect (up to 18°N). The flux ratio increased from ~13:1 to a maximum in the CIO of ~ 17.1 at 5.5°N, and then declined linearly to minimum of 13.2 \pm 0.17 between 14.5-16.5°N in the IMG. Nitrate and phosphate concentrations were below the detection limit (0.05 µmol L⁻¹) in the top 40 m, with the exception of one point at 6.5°N (Figure 4). Below the nutricline (115 \pm 36

m) and down to 200 m depth in the ISSG, nitrate concentrations remained less than 3.5 umol L⁻¹. In the CIO and IMG, where the nutricline shoaled to 75 m or less, nitrate concentrations were generally above 20 umol L⁻¹ in the region between the nutricline and 200 m depth. Phosphate concentrations followed a similar pattern to nitrate, with values below the nutricline (but above 200 m) approximately 0.3 µmol L⁻¹ in the ISSG, gradually increasing through the south-to-north transect of the CIO (1.6 \pm 0.19 μ mol L⁻¹) and IMG (2.0 \pm 0.27 μ mol L⁻¹). Dissolved N:P (mol:mol) ratios, unlike N:P flux ratios, were constrained between 9-11.5 from 28°S to 17°S, and increased to 13-15 for the remainder of the transect north of 17°S in the waters below the nutricline (Figure 4). The difference between flux ratios and stock concentration ratios highlights the importance of the nutrient gradients below the nutricline. Ammonium concentrations were below the detection limit (0.05 µmol N L⁻¹) throughout the transect, with the exception of localized concentrations of ~0.24 umol L⁻¹ between the depths of 60 and 80 m from 2.8°S-5.0°N. Urea concentrations in the ISSG were 0.04 µmol L⁻¹ and gradually increased to a maximum of 0.18 µmol L⁻¹ in the IMG (Table 1). There was not much variability in DOP concentrations, with an average and standard deviation of $0.31 \pm 0.04 \,\mu\text{mol L}^{-1}$ over the entire transect.

3.2 Phytoplankton

272

273

274

275

276

277

278

279

280

281

282

283

284

285

286

287

288

289

290

291

292

293

294

Chl *a* concentrations at 20m depth were highest at values 0.12 to 0.20 mg m⁻³ between the equator and 6.5°N (Table 1). A subsurface chlorophyll maximum (data not shown) was observed between 50-85m in the CIO and IMG, with concentrations 4-7 times those found at 20m. Cell counts and living biomass (μ g C L⁻¹) were dominated by the smallest organisms, namely heterotrophic bacteria and autotrophic *Prochlorococcus* (Table 1, Figure 5), with significantly (p<0.01) higher numbers (>200 x10³ cells ml⁻¹) and biomass (>6.5 μ g C L⁻¹) found

in the CIO. Throughout the study region, *Prochlorococcus* accounted for $78 \pm 6.3\%$ of autotrophic biomass. *Synechococcus* populations were two orders of magnitude less numerous, and almost non-existent (<1000 cells ml⁻¹) in the surface ISSG. *Synechococcus* abundance (Table 1) and biomass (Figure 5) reached its highest values within a few degrees of the equator. Small eukaryotes (<20 μ m) were an order of magnitude less numerous compared to cyanobacteria throughout our study region. In terms of biomass, small eukaryotes constituted 20 \pm 11% of autotrophic biomass over the entire transect. Larger eukaryotes (e.g. diatoms, dinoflagellates) were rare (generally <10 cells L⁻¹), with a mean biomass of 0.14 \pm 0.13 μ g C L⁻¹, which is approximately 1.5% of the total autotrophic biomass.

3.3 Carbon and Nitrogen Uptake

Community uptake rates for all compounds tested (HCO₃, NO₃, NH₄, and urea) were significantly greater in the CIO and IMG when compared to rates in the ISSG (student's t-tests; p<0.001). Nitrate uptake rates had an overall mean and standard deviation of 1.3 ± 0.9 nmol L⁻¹ h⁻¹ in the ISSG. Rates generally increased from south to north through the CIO and IMG (Figure 6). Ammonium uptake rates averaged 1.8 ± 0.9 nmol L⁻¹ h⁻¹ in the ISSG increased to an average of 6.3 ± 1.3 nmol L⁻¹ h⁻¹ in the CIO and then decreased (p=0.08) to 5.3 ± 1.2 nmol L⁻¹ h⁻¹ in the IMG. The f-ratio (0.20 ± 0.06) showed little variation through the entire IO transect (Figure 6), although the mean f-ratio did trend slightly positive from the ISSG (0.17 ± 0.04) to the CIO (0.21 ± 0.05) and IMG (0.20 ± 0.09). The maximum f-ratios (0.27 ± 0.06) were found between $1.5-8.0^{\circ}$ N. Urea uptake rates were significantly lower (p<0.01) in the ISSG, with a mean of 0.93 ± 0.87 nmol L⁻¹ h⁻¹, and higher in the CIO (4.9 ± 2.7 nmol L⁻¹ h⁻¹) and in the IMG (6.2 ± 1.9 nmol L⁻¹ h⁻¹). Maximum uptake rates (mean of 1.4, 3.9, and 6.3 nmol L⁻¹ h⁻¹; n=5) for nitrate, ammonium and urea respectively) were found between $1.5-8.0^{\circ}$ N, the same location as a

potential upwelling where the nutricline shoals to the shallowest depth found along the transect and nutrient fluxes were calculated to be highest (Lee, 2004).

Total community inorganic carbon uptake followed a similar pattern as nitrogen uptake rates, with a generally increasing trend from the south to the north. The ISSG had significantly lower (p<0.001) C uptake rates $(1.7 \pm 1.4 \text{ nmol L}^{-1} \text{ h}^{-1})$ than the CIO $(6.3 \pm 2.4 \text{ nmol L}^{-1} \text{ h}^{-1})$ and IMG $(5.7 \pm 1.9 \text{ nmol L}^{-1} \text{ h}^{-1})$. Maximum average rates of 8.6 nmol C L⁻¹ h⁻¹ were observed between 1.5-6.5°N (Figure 6). The C:NO₃ uptake rate ratio (mol:mol) was not significantly different (p>0.2) between the regions, with a mean and standard deviation across the transect of 4.2 ± 1.8 (Figure 6). If NH₄ is also included in C:N uptake ratio calculations, the ratio for all stations decreases to 0.77 ± 0.22 .

Uptake rate calculations are sensitive to ambient substrate concentrations. Because all measurements of nitrate and ammonium concentrations were below detection limit (50 nmol L^{-1}) we assumed ambient concentrations to be half (25 nmol L^{-1}) of that limit. Compared to what the rates would have been if we had assumed an ambient concentration of zero, absolute nitrate and ammonium uptake rates increased by 0.73 ± 0.42 and 2.3 ± 1.1 nmol L^{-1} h⁻¹ respectively. Most ambient urea concentrations were measurable (Table 1), but at the few locations where concentrations were below the detection limit, the same correction was applied, half of the detection limit is 5 nmol L^{-1} , resulting in an increase in urea uptake rates of 0.86 ± 1.1 nmol L^{-1} h⁻¹.

The rates reported in this study were potentially underestimated given the dominance by *Prochlorococcus* and the use of GF/F filters (0.7 µm nominal pore size), which may allow some portion of the smallest cells to pass through. However, prior studies have found less than 5% of *Prochlorococcus* cells would be lost using this method (Chavez et al., 1995). On the other hand,

increases in temperature can inflate rates of uptake. Incubations utilizing the on-deck flow-through system struggled to maintain ambient sea surface temperatures. Mean temperatures in the incubation bottles were 1.0 ± 0.71 °C above ambient, while maximum temperatures were 2.0 ± 0.80 °C above ambient (Figure S1). Given a Q_{10} of ~2 for both carbon and nitrogen uptake (e.g. Berges et al., 2002; Lomas et al., 2002; Sherman et al., 2016) would represent a 10-20% increase in uptake rates, suggesting this is of larger concern than cells passing the GF/F filter.

4 Discussion

Carbon and nitrogen productivity and phytoplankton community data in the oligotrophic central IO are limited. Published measurements of plankton and biogeochemical rates are mostly restricted to the eastern IO near coastal Australia, the Indian section of the Southern ocean and the JGOFS program in the Arabian Sea (e.g. Naqvi, 2008), all of which are subject to very different physical forcing and chemical environments than the central IO along 95°E, where our transect took place. That said, given our understanding of the physical and nutrient regime from prior GO-SHIP hydrography transects, we expect some large-scale patterns to emerge. This study provides a "baseline" description of the regional oceanographic conditions and integration with corresponding variation in phytoplankton biodiversity and biogeochemical rates in the vast oligotrophic IO.

4.1 Physics and nutrients

The oligotrophic IO is a strongly stratified system, with high temperatures (>25°C) found throughout most of the surface 50 m (Figure 2) due to local surface heating, and not likely to be influenced by the IO dipole mode (Saji et al., 1999), which had no anomaly during our cruise

time frame (see: http://stateoftheocean.osmc.noaa.gov/sur/ind/dmi.php). There are significant freshwater inputs sourced from the Indonesian Through-Flow and rivers surrounding the Bay of Bengal, which causes significant freshening, and further stratification of surface waters north of the equator (Schott and McCreary Jr., 2001; Sengupta et al., 2006). The area between 12-28°S is a traditional oceanic gyre, where the nutricline is deeper due to overturning circulation that causes downwelling (Lee, 2004). Because of the high surface temperatures and freshening waters in the north (Figure 2), stratification was very high, with a sharp nutricline and little to no measurable nutrients in the surface waters (Figure 4). North of 12°S, in the CIO and IMG, the mixed layer was restricted to 50 m depth, with multiple stations where it shoaled within 20m of the surface (Figure 3). Nutricline depth in the ISSG was almost always >100 m. In the CIO and IMG, the nutricline averaged 65 m. Between 4-6°N there was a shallow nutricline (<50 m), with minimal depth difference between the mixed layer and nutricline depths. These physical processes appear to shape the ecosystem, describing the three biogeochemical zones we defined along the transect (ISSG, CIO, and IMG).

Macronutrients were constrained to below the mixed layer depth, with increasing concentrations from south-to-north (Figure 4). We used a flux calculation to understand the magnitude of both nitrate and phosphate entering the euphotic zone, where our incubations took place. The fluxes increased from south-to-north, but not at the same rate for nitrate and phosphate, leading to a peak in the ratio of dissolved N:P flux (>17) at approximately 5°S, progressively becoming a smaller ratio (down to ~13) moving either north of south of that location, with most values below the Redfield ratio of 16. Using the flux ratio (Figure 3), rather than the ratio of absolute concentrations (Figure 4), gives a very different picture of the nutrient status of the three regions. While the low absolute values of dissolved inorganic nutrients

indicate a generally nutrient stressed system, it appears to be that nitrate is the proximate limiting nutrient, relative to Redfield ratio.

Measurements of organic N (urea) and dissolved organic P (DOP) were consistently greater than inorganic N and P forms (Table 1). Consistent with prior studies (Prakash et al., 2015), urea is an important contributor to N nutrition for autotrophic organisms in this area. While nitrate is supplied through vertical exchange with the ocean interior, the source of urea is not clear. Generally, sloppy feeding, bacterial and microzooplankton regeneration, and phytoplankton exudation are likely origin candidates (Bronk and Steinberg, 2008). Additionally, small autotrophic cells (such as cyanobacteria) have been shown to release urea, even when N limited (Hasegawa et al., 2000). Rates of bacterial urea production, resulting from amino acid degradation, can meet phytoplankton N demand, at least in coastal waters (Cho et al., 1996), but it is not clear to what extent this process is present in this gyre system. While there are a number of potential urea sources, they remain to be quantified and their importance shown in this system.

Concentrations of DOP were consistently greater than phosphate throughout the region (Table 1; $0.31~\mu mol~L^{-1}$ mean for the entire transect), and generally higher than the N. Atlantic subtropical gyre, which have been reported to be between $0.06\text{-}0.08~\mu mol~L^{-1}$ in the spring (Lomas et al., 2010; Mather et al., 2008). With low inorganic P concentrations, microorganisms may utilize DOP as their primary P source, which may help explain the observation that particulate C:P values were only slightly higher than Redfield for most of the transect (Garcia et al., in review) . Dissolved organic carbon (DOC) concentrations reported from prior cruises in this region (see Hansell (2009); data available at https://www.nodc.noaa.gov/ocads/oceans/RepeatSections/clivar_i09n.html) indicate that the IO has similar DOC stocks (60-70 μ mol L⁻¹) compared to other major ocean basins (Carlson, 2002).

Ratios of DOC:DOP in the oligotrophic IO (mean of 215:1), while still higher than both Redfield and particulate forms in this system, were much lower than the ratio of ~1200:1 found in the North Atlantic gyre at BATS (Singh et al., 2015). Although speculative, the potential reduction in phosphorus stress within the IO is likely to cause active cycling of organic compounds in this region, as shown below with urea uptake rates and calculated growth rates.

4.2 Plankton Abundance and Biomass

409

410

411

412

413

414

415

416

417

418

419

420

421

422

423

424

425

426

427

428

429

430

431

Prior studies of autotrophs in the equatorial IO (Sorokin et al., 1985) and the Bay of Bengal (Madhupratap et al., 2003) have focused on total chl a concentrations or larger (>5 μm) eukaryotes. One recent study found abundant evidence of single-cell cyanobacteria expressing high-light and nutrient-stress genes (Díez et al., 2016) and *Prochlorococcus* tends to be found where temperatures are high and nutrients are low (Flombaum et al., 2013). Consistent with this observation, we found that autotrophic surface biomass in the entire IO including the Bay of Bengal was dominated by *Prochlorococcus* (Figure 5). Synechococcus, while co-occurring, was found at much lower cell abundances, similar to the relative abundances of *Prochlorococcus* and Synechococcus found in the Pacific gyre (Karl and Church, 2014). Where the mixed layer was deeper and closer to the nutricline around the equator (Figure 3), Synechococcus were more numerous (Figure 5). In the Sargasso Sea, Synechococcus reaches a seasonal maximum during winter/spring convection when nitrate inputs are highest (Casey et al., 2013; DuRand et al., 2001). In the Pacific gyre, *Prochlorococcus* appears to be better adapted to a high-light and low iron regime than *Synechococcus* (Partensky et al., 1999), and it seems likely that the same environmental conditions are shaping the phytoplankton community in the surface oligotrophic IO during the spring intermonsoon season conditions sampled during the present study. In the IMG and the southern ISSG, N:P diffusive flux ratios were low (≤14; Figure 3) and therefore P-

rich, which corresponded to lower relative Prochlorococcus biomass, although the correlation between Prochlorococcus biomass and the N:P flux ratio (r = 0.470) was not statistically significant.

432

433

434

435

436

437

438

439

440

441

442

443

444

445

446

447

448

449

450

451

452

453

Eukaryotic autotrophs, especially larger organisms (>20 μm) such as diatoms and dinoflagellates, were found at low levels along the entire transect (<2% of total biomass). Autotrophic nanoplankton (<20 μm) also were found at consistently low abundance (Table 1) and biomass (Figure 5) but were a higher proportion of the overall plankton community in the ISSG than the other regions. In the northern ISSG, relatively high nanoplankton biomass was found in the same area of highest dissolved N:P flux ratios (Figure 3), potentially indicating a release from N-stress that these organisms can exploit. Outside of that region, N-fixers would be expected but were not readily detected along our transect. Trichosdesmium has been found seasonally in the Bay of Bengal and along the coasts, but is not commonly observed in the open waters of the central IO (Hegde et al., 2008). In the oligotrophic IO, far from terrestrial sources of dust, N-fixer biomass and growth could be limited by iron stress (Grand et al., 2015). However, it is entirely possible that we didn't observe N-fixers because we were not explicitly looking for them, or that they were not abundant during the spring season when the sampling took place. Hegde et al. (2008) noted the suddenness with which Trichodesmium in coastal systems blooms and declines.

Heterotrophic bacterial biomass was correlated (r=0.721; p<0.001) with autotrophic biomass (Figure 5). Prior studies in the equatorial region of the IO have found bacterial production to be greater than primary production (Fernandes et al., 2008). While our study did not measure bacterial production specifically, the low inorganic nutrient concentrations and high

bacterial biomass implies a strong microbial loop in this region, especially when considering that the phytoplankton community is a likely source of semi-labile DOC (Hansell, 2009).

4.3 Autotrophic production

454

455

456

457

458

459

460

461

462

463

464

465

466

467

468

469

470

471

472

473

474

475

476

Rates of primary production (0.12 – 12.4 nmol C L⁻¹ h⁻¹) were lower than those measured in other oligotrophic gyres, which tend to be above 20 nmol C L⁻¹ h⁻¹ (e.g. Williams et al., 2013). Maximum primary productivity rates (absolute C uptake; Figure 6) were found at approximately 6°N. Absolute fluxes of dissolved nutrients (>0.9 umol N m⁻² d⁻¹ and >0.6 umol P m⁻² d⁻¹) were further north in the Bay of Bengal, but at a lower N:P flux ratio (<14.5; Figure 3). There was a combination of high nutrient fluxes along with high diffusive N:P flux ratios at 6°N, and the community appeared to be primed to respond to this relatively N-rich physico-chemical regime. Biomass increased in relation to shallower mixed layer and nutricline depths, and absolute C uptake was correlated to increased biomass (r = 0.601; p<0.01). There are a few stations where C uptake rates were higher than predicted by a linear relationship to biomass (Figure 8). The limited studies of microzooplankton in the IO indicate that grazer abundances are high (Sorokin et al., 1985). High grazing rates, along with high nutrient remineralization could lead to deviations from the biomass to C uptake relationship. On the opposite end of the spectrum, in the ISSG nutrient fluxes were low (<0.16 µmol N m⁻² d⁻¹ and <0.01 µmol P m⁻² d⁻¹), diffusive N:P flux rates were low but highly variable, and subsequently little biomass (<5 ug C L⁻¹ total autotrophic biomass) and low C uptake rates (<6 nmol C L⁻¹ h⁻¹). Rates of absolute N uptake increased from south-to-north, with a peak in rates found north of the equator to 8°N. The same region (i.e. 1.5-8.0°N) has the least difference in depth between the mixed layer and nutricline depths (Figure 3). Similar to a study in the equatorial region of the IO (Prakash et al., 2015), N uptake of NO₃ and NH₄ were less than 10 nmol N L⁻¹

h⁻¹ but with a surprisingly high high f-ratio (mean = 0.23 ± 0.04 ; Figure 6) compared to other oligtrophic gyres, where the f-ratio is generally <0.10 (Eppley and Peterson, 1979; Lipschultz, 2001). The high f-ratios could be because there is little ammonium in the system to support high rates. While we think of oligotrophic regions as regenerative systems, we would also expect to find some ammonium signal in the ambient dissolved nutrient concentrations. It is possible that the community is taking up the ammonium as fast as it is produced, or that ammonium is a reduced resource and the autotrophic community is primed to use either nitrate or other organic nutrients.

The ratio of carbon:nitrate uptake was generally below 2.0 throughout the study region, substantially below the canonical Redfield ratio of 6.6 (Figure 6), suggesting that the autotrophic community is not limited by N resources. This is likely due to the presence of organic N forms found in this study that can be readily assimilated. Bulk particulate C:N in the IO had a mean value of 7.1 with no significant differences between the three defined regions (Garcia et al., in review). This ratio however includes detritus and non-autotrophic biomass.

N uptake rates were highest in the organic N form we studied (urea). Urea is not typically used as a substrate in N uptake rate experiments in the oligotrophic gyres, but our findings show that organic N is a critical resource in this oligotrophic system. We are unable to distinguish whether there are specific members of the community utilizing the different N compounds. *Prochlorococcus* are known to use organic forms of N (Casey et al., 2007; Rocap et al., 2003; Zubkov et al., 2003). Alternatively, it could be that both ammonium and urea are being utilized primarily by heterotrophic bacteria, which could be caught on our filters. Prior studies have shown that up to 80% of bacterial community members can be retained on GF/F filters (Bradley et al., 2010; Fouilland et al., 2007). Therefore, up to 28% of the measured

ammonium and urea uptake rates could be due to bacterial activity, corresponding to a mean and standard deviation of 1.1 ± 0.52 and 0.96 ± 0.66 nmol N L⁻¹, respectively.

500

501

502

503

504

505

506

507

508

509

510

511

512

513

514

515

516

517

518

519

520

521

522

Using a compilation of cruise results, Hansell (2009) found an elevated DOC signal in the ISSG that was not readily explained by physical processes. We found higher than expected carbon uptake and growth rates in the ISSG (Figures 6 and 7). Primary production was decoupled from nitrogen uptake, as evidenced by the low C:N ratio of uptake rates (4.1) compared to the C:N of particles (mean of 7.1 along the IO transect; Garcia et al., in review). Additionally, this carbon taken up does not appear to be accumulating in particles, as biomass was relatively low, and the particulate C:N ratios were lower than the C:N of uptake. Given full transect mean growth rates of 0.24 ± 0.12 d⁻¹, particulate biomass C:N ratio of 7.1, and C:N uptake ratio of 4.1 ± 1.7 , DOC is likely accumulated locally from phytoplankton production and release. DOC production rates can be estimated from the difference between absolute C uptake rates (Figure 6) and the product of biomass (Figure 5) and growth rates (Figure 7). Assuming a surface value of 65 µmol L⁻¹ of DOC (Hansell, 2009), turnover times of DOC in the surface IO average 650 ± 626 , 194 ± 129 , and 38 ± 3 d in the ISSG, CIO, and IMG respectively. As stated above, the dissolved organic matter in the oligotrophic IO as a whole was relatively enriched in phosphorus. It is therefore surprising that DOC can accumulate in this region at all, especially given the high bacterial production rates found in the central IO (Fernandes et al., 2008), although it is possible that bacterial respiration is limited by the high temperatures found in the surface waters found at lower latitudes (López-Urrutia and Morán, 2007). More research is needed to explain the relationships between primary and secondary production in the oligotrophic IO, and the decoupling of carbon and nitrogen biogeochemical cycles found there.

524

525

526

527

528

529

530

531

532

533

534

535

536

537

538

539

540

541

542

543

544

545

4.4 Regional summary

The central oligotrophic IO has had limited direct observations of biogeochemical parameters. Based on what was known of physical conditions and nutrient concentrations, we hypothesized three distinct biogeochemical zones, although our observations did not fully support this hypothesis. In the ISSG, we expected typical gyre conditions, with intermediate temperatures, low total nitrogen, and low iron availability, the combination of which would lead to a predominance of single cell cyanobacteria. While *Prochlorococcus* biomass was higher than other taxa, it made up a lower percentage of total biomass in the ISSG than the CIO and IMG. This is likely due to low dissolved N and P fluxes (Figure 3) limiting the growth of the plankton community overall. The southern ISSG showed a suppression of biomass but not a slowing down of physiology, as growth rates were still a mean of 0.13 in the ISSG (Figure 7). This decoupling of the carbon and nitrogen cycles potentially leads to a highly labile and abundant pool of organic matter. In the CIO, we encountered increasing nutrient concentrations below the nutricline and dissolved N:P fluxes entering the surface 50m, along with higher temperatures. These physical and chemical conditions were coincident with higher uptake rates and biomass increases. While we expected the trend for increasing uptake rates and biomass to continue into the IMG, but it did not. In the IMG, primary production and nitrogen uptake were lower on average than the CIO. Moving further north within the IMG into the Bay of Bengal, carbon uptake rates decreased further, potentially due to N limitation (N:P flux ratios <14) and the increased difference between mixed layer and nutricline depths. Throughout the oligotrophic IO, organic matter cycling is very dynamic and a potential avenue for further study.

This data set will inform remote sensing and modeling work in this relatively understudied region of the global ocean. Future work is needed to understand the biogeochemistry in other seasons and throughout the euphotic zone. Furthermore, how primary production and biomass relates to export in the different regions of the oligotrophic IO will be critical for a better understanding of global C cycling.

Acknowledgments

We wish to thank the GO-SHIP repeat hydrography program, Captain Curl and the crew of the R/V Roger Revelle. The chief scientists, Leticia Barbero and Carmen Rodriguez, ensured smooth operations. The UCSD ODF team, led by Susan Becker, provided nutrient data. Many thanks to Norm Nelson and Jeremy Kravitz for chlorophyll *a* analyses and data, Abraham Steinberger for help with flow cytometry, and Laura Lubelczyk for assistance with FlowCAM operation and analysis. This work was supported by the National Science Foundation [grant numbers OCE-1559021 (MWL, BST), OCE-xxxxxx (ACM)].

Disclosures

SEB, SR, and CAG conducted the research. SEB analyzed the data and wrote the manuscript. ACM, BST and MWL conceived of the research and all authors edited the manuscript. All authors have approved the final article. Conflicts of interest: none.

References

- Alory, G., Meyers, G., 2009. Warming of the upper equatorial Indian Ocean and changes in the heat budget (1960-1999). J. Clim. 22, 93–113.
- Behrenfeld, M.J., Falkowski, P.G., 1997. Photosynthetic rates derived from satellite-based chlorophyll concentration. Limnol. Oceanogr. 42, 1–20.
- Behrenfeld, M.J., O'Malley, R.T., Siegel, D.A., McClain, C.R., Sarmiento, J.L., Feldman, G.C.,

- Milligan, A.J., Falkowski, P.G., Letelier, R.M., Boss, E.S., 2006. Climate-driven trends in contemporary ocean productivity. Nature 444, 752–755.
- Berges, J.A., Varela, D.E., Harrison, P.J., 2002. Effects of temperature on growth rate, cell composition and nitrogen metabolism in the marine diatom Thalassiosira pseudonana (Bacillariophyceae). Mar. Ecol. Prog. Ser. 225, 139–146.
- Bianchi, M., Feliatra, F., Tréuger, P., Vincendeau, M.-A., Morvan, J., 1997. Nitrification rates, ammonium and nitrate distribution in upper layers of the water column and in sediments of the Indian sector of the Southern Ocean. Deep Sea Res. Part II Top. Stud. Oceanogr. 44, 1017–1032. https://doi.org/http://dx.doi.org/10.1016/S0967-0645(96)00109-9
- Bouman, H.A., Ulloa, O., Scanlan, D.J., Zwirglmaier, K., Li, W.K.W., Platt, T., Stuart, V.,
 Barlow, R., Leth, O., Clementson, L., Lutz, V., Fukasawa, M., Watanabe, S.,
 Sathyendranath, S., 2006. Oceanographic basis of the global surface distribution of
 Prochlorococcus ecotypes. Science (80-.). 312, 918–921.
 https://doi.org/10.1126/science.1122692
- Boyce, D.G., Lewis, M.R., Worm, B., 2010. Global phytoplankton decline over the past century.
 Nature 466, 591–596.
- Bradley, P.B., Lomas, M.W., Bronk, D.A., 2010. Inorganic and organic nitrogen use by
 phytoplankton along Chesapeake Bay, measured using a flow cytometric sorting approach.
 Estuaries and Coasts 33, 971–984. https://doi.org/DOI 10.1007/s12237-009-9252-y
 Brewin, R.J.W., Hirata, T., Hardman-Mountford, N.J., Lavender, S.J., Sathyendranath, S.,
 - Brewin, R.J.W., Hirata, T., Hardman-Mountford, N.J., Lavender, S.J., Sathyendranath, S., Barlow, R., 2012. The influence of the Indian Ocean Dipole on interannual variations in phytoplankton size structure as revealed by Earth Observation. Deep Sea Res. Part II Top. Stud. Oceanogr. 77–80, 117–127. https://doi.org/10.1016/J.DSR2.2012.04.009
- Bronk, D.A., Steinberg, D.K., 2008. Nitrogen regeneration, in: Capone, D.G., Bronk, D.A.,
 Mulholland, M.R., Carpenter, E.J. (Eds.), Nitrogen in the Marine Environment. Elsevier
 Inc., San Diego, CA, pp. 385–467.

591

- Carlson, C.A., 2002. Production and removal processes, in: Hansell, D.A., Carlson, C.A. (Eds.),
 Biogeochemistry of Marine Dissolved Organic Matter. Academic Press, San Diego, pp. 91–
 151.
- Casey, J.R., Aucan, J.P., Goldberg, S.R., Lomas, M.W., 2013. Changes in partitioning of carbon amongst photosynthetic pico- and nano-plankton groups in the Sargasso Sea in response to changes in the North Atlantic Oscillation. Deep Sea Res. Part II Top. Stud. Oceanogr. 93, 58–70.
- 603 Casey, J.R., Lomas, M.W., Mandecki, J., Walker, D.E., 2007. *Prochlorococcus* contributes to new production in the Sargasso Sea deep chlorophyll maximum. Geophys. Res. Lett. 34, L10604, doi:10.1029/2006GL028725.
- Cermeño, P., Dutkiewicz, S., Harris, R.P., Follows, M., Schofield, O., Falkowski, P.G., 2008.
 The role of nutricline depth in regulating the ocean carbon cycle. Proc. Natl. Acad. Sci. 105, 20344–20349. https://doi.org/10.1073/pnas.0811302106
- Chavez, F.P., Buck, K.R., Bidigare, R.R., Karl, D.M., Hebel, D., Latasa, M., Campbell, L., 1995.
 On the chlorophyll a retention properties of glass-fiber GF/F filters. Limnol. Oceanogr. 40,
 428–433.
- Cho, B.C., Park, M.G., Shim, J.H., Azam, F., 1996. Significance of bacteria in urea dynamics in coastal surface waters. Mar. Ecol. Prog. Ser. 142, 19–26.
- Dickson, A.G., Sabine, C.L., Christian, J.R., 2007. Guide to best practices for ocean CO2 measurements.

- Díez, B., Nylander, J.A.A., Ininbergs, K., Dupont, C.L., Allen, A.E., Yooseph, S., Rusch, D.B.,
 Bergman, B., 2016. Metagenomic analysis of the Indian Ocean picocyanobacterial
 community: Structure, potential function and evolution. PLoS One 11, e0155757.
 https://doi.org/10.1371/journal.pone.0155757
- Duarte, C.M., Cebrián, J., 1996. The fate of marine autotrophic production. Limnol. Oceanogr. 41, 1758–1766.
- Dugdale, R.C., Goering, J.J., 1967. Uptake of new and regenerated forms of nitrogen in primary productivity. Limnol. Oceanogr. 12, 196–206.
- DuRand, M.D., Olson, R.J., Chisholm, S.W., 2001. Phytoplankton population dynamics at the Bermuda Atlantic Time-series station in the Sargasso Sea. Deep Sea Res. Part II Top. Stud. Oceanogr. 48, 1983–2003.
- Eppley, R.W., Peterson, B.J., 1979. Particulate organic matter flux and planktonic new production in the deep ocean. Nature 282, 677–680. https://doi.org/doi:10.1038/282677a0

630

- Fernandes, V., Rodrigues, V., Ramaiah, N., Paul, J.T., 2008. Relevance of bacterioplankton abundance and production in the oligotrophic equatorial Indian Ocean. Aquat. Ecol. 42, 511–519. https://doi.org/10.1007/s10452-007-9142-y
- Flombaum, P., Gallegos, J.L., Gordillo, R.A., Rincóna, J., Zabala, L.L., Jiao, N., Karl, D.M., Lie,
 W.K.W., Lomas, M.W., Veneziano, D., Vera, C.S., Vrugt, J.A., Martiny, A.C., 2013.
 Present and future global distributions of the marine Cyanobacteria Prochlorococcus and
 Synechococcus. Proc. Natl. Acad. Sci. USA 110, 9824–9829.
- Fouilland, E., Gosselin, M., Rivkin, R.B., Vasseur, C., Mostajir, B., 2007. Nitrogen uptake by
 heterotrophic bacteria and phytoplankton in Arctic surface waters. J. Plankton Res. 29, 369–376.
- Fukuda, R., Ogawa, H., Nagata, T., Koike, I., 1998. Direct determination of carbon and nitrogen
 contents of natural bacterial assemblages in marine environments. Appl. Environ.
 Microbiol. 64, 3352–3358.
- Garcia, C.A., Baer, S.E., Garcia, N.S., Rauschenberg, S., Twining, B.S., Lomas, M.W., Martiny,
 A.C., n.d. Nutrient supply controls particulate elemental concentrations and ratios in the
 eastern Indian Ocean.
- Garrison, D.L., Gowing, M.M., Hughes, M.P., Campbell, L., Caron, D.A., Dennett, M.R.,
 Shalapyonok, A., Olson, R.J., Landry, M.R., Brown, S.L., Liu, H.-B., Azam, F., Steward,
 G.F., Ducklow, H.W., Smith, D.C., 2000. Microbial food web structure in the Arabian Sea:
 a US JGOFS study. Deep Sea Res. Part II Top. Stud. Oceanogr. 47, 1387–1422.
 https://doi.org/10.1016/S0967-0645(99)00148-4
- Goeyens, L., Kindermans, N., Abu Yusuf, M., Elskens, M., 1998. A room temperature procedure for the manual determination of urea in seawater. Estuar. Coast. Shelf Sci. 47, 415–418.
- Grand, M.M., Measures, C.I., Hatta, M., Hiscock, W.T., Landing, W.M., Morton, P.L., Buck,
 C.S., Barrett, P.M., Resing, J.A., 2015. Dissolved Fe and Al in the upper 1000 m of the
 eastern Indian Ocean: A high-resolution transect along 95°E from the Antarctic margin to
 the Bay of Bengal. Global Biogeochem. Cycles 29, 375–396.
 https://doi.org/10.1002/2014GB004920
- Hama, T., Miyazaki, T., Ogawa, Y., Iwakuma, T., Takahashi, M., Otsuki, A., Ichimura, S., 1983.
 Measurement of photosynthetic production of a marine phytoplankton population using a stable 13C isotope. Mar. Biol. 73, 31–36.
- Hansell, D.A., 2009. Dissolved organic carbon in the carbon cycle of the Indian Ocean, in:
 Wiggert, J.D., Hood, R.R., Naqvi, S.W.A., Brink, K.H., Smith, S.L. (Eds.), Indian Ocean

- Biogeochemical Processes and Ecological Variability. AGU Geophysical Monograph Series, pp. 217–230.
- Hasegawa, T., Koike, I., Mukai, H., 2000. Release of dissolved organic nitrogen by sizefractionated natural planktonic assemblages in coastal waters. Mar. Ecol. Prog. Ser. 198, 43–49.
- Hegde, S., Anil, A.C., Patil, J.S., Mitbavkar, S., Krishnamurthy, V., Gopalakrishna, V. V, 2008.
 Influence of environmental settings on the prevalence of Trichodesmium spp. in the Bay of
 Bengal. Mar. Ecol. Prog. Ser. 356, 93–101.
- Hood, R.R., Wiggert, J.D., Naqvi, S.W.A., 2009. Indian Ocean biogeochemical process and
 ecological variability, in: Indian Ocean Research: Opportunities and Challenges. American
 Geophysical Union.
- Hydes, D., Aoyama, M., Aminot, A., Bakker, K., Becker, S., Coverly, S., Daniel, A., Dickson,
 A.G., Grosso, O., Kerouel, R., van Ooijen, J., Sato, K., Tanhua, T., Woodward, E.M.S.,
 Zhang, J.Z., 2010. Determination of dissolved nutrients (N, P, Si) in seawater with high
 precision and inter-comparability using gas-segmented continuous flow analysers, in: Hood,
 E.M., Sabine, C.L., Sloyan, B.M. (Eds.), The GO-SHIP Repeat Hydrography Manual
 IOCCP Report. pp. 1–87.
- Karl, D.M., Church, M.J., 2014. Microbial oceanography and the Hawaii Ocean Time-series programme. Nat. Rev. Microbiol. 12, 699–713. https://doi.org/10.1038/nrmicro3333
- Kumar, S., Ramesh, R., Sardesai, S., Sheshshayee, M.S., 2004. High new production in the Bay
 of Bengal: Possible causes and implications. Geophys. Res. Lett. 31, L18304,
 doi:10.1029/2004GL021005. https://doi.org/10.1029/2004GL021005
- Lee, T., 2004. Decadal weakening of the shallow overturning circulation in the South Indian
 Ocean. Geophys. Res. Lett. 31, L18305, doi:10.1029/2004GL020884.
 https://doi.org/10.1029/2004GL020884

690

691

692

693

694

- Lipschultz, F., 2001. A time-series assessment of the nitrogen cycle at BATS. Deep. Res. Part II-Topical Stud. Oceanogr. 48, 1897–1924.
 - Lomas, M.W., Burke, A.L., Lomas, D.A., Bell, D.W., Shen, C., Dyhrman, S.T., Ammerman, J.W., 2010. Sargasso Sea phosphorus biogeochemistry: an important role for dissolved organic phosphorus (DOP). Biogeosciences 7, 695–710. https://doi.org/10.5194/bg-7-695-2010
 - Lomas, M.W., Glibert, P.M., Shiah, F.-K., Smith, E.M., 2002. Microbial processes and temperature in Chesapeake Bay: current relationships and potential impacts of regional warming. Glob. Chang. Biol. 8, 51–70.
- López-Urrutia, Á., Morán, X.A.G., 2007. Resource limitation of bacterial production distorts the
 temperature dependence of oceanic carbon cycling. Ecology 88, 817–822.
 https://doi.org/doi:10.1890/06-1641
- Madhupratap, M., Gauns, M., Ramaiah, N., Prasanna Kumar, S., Muraleedharan, P.M., de Sousa,
 S.N., Sardessai, S., Muraleedharan, U., 2003. Biogeochemistry of the Bay of Bengal:
 physical, chemical and primary productivity characteristics of the central and western Bay
 of Bengal during summer monsoon 2001. Deep Sea Res. Part II Top. Stud. Oceanogr. 50,
 881–896. https://doi.org/http://dx.doi.org/10.1016/S0967-0645(02)00611-2
- Mahowald, N.M., Baker, A.R., Bergametti, G., Brooks, N., Duce, R.A., Jickells, T.D., Kubilay,
 N., Prospero, J.M., Tegen, I., 2005. Atmospheric global dust cycle and iron inputs to the
 ocean. Global Biogeochem. Cycles 19.
- Marie, D., Partensky, F., Jacquet, S., Vaulot, D., 1997. Enumeration and cell cycle analysis of

- natural populations of marine picoplankton by flow cytometry using the nucleic acid stain SYBR Green I. Appl. Environ. Microbiol. 63, 186–193.
- Martiny, A.C., Huang, Y., Li, W., 2009. Occurrence of phosphate acquisition genes in
 Prochlorococcus cells from different ocean regions. Environ. Microbiol. 11, 1340–1347.
 https://doi.org/10.1111/j.1462-2920.2009.01860.x
- Mather, R.L., Reynolds, S.E., Wolff, G.A., Williams, R.G., Torres-Valdes, S., Woodward, E.M.S., Landolfi, A., Pan, X., Sanders, R., Achterberg, E.P., 2008. Phosphorus cycling in the North and South Atlantic Ocean subtropical gyres. Nat. Geosci. 1, 439–443.
- Menden-Deuer, S., Lessard, E.J., 2000. Carbon to volume relationships for dinoflagellates, diatoms, and other protist plankton. Limnol. Oceanogr. 45, 569–579.
- Morrison, J.., Codispoti, L.., Gaurin, S., Jones, B., Manghnani, V., Zheng, Z., 1998. Seasonal variation of hydrographic and nutrient fields during the US JGOFS Arabian Sea Process
 Study. Deep Sea Res. Part II Top. Stud. Oceanogr. 45, 2053–2101.
 https://doi.org/10.1016/S0967-0645(98)00063-0
- Naqvi, S.W.A., 2008. The Indian Ocean, in: Capone, D.G., Bronk, D.A., Mulholland, M.R.,
 Carpenter, E.J. (Eds.), Nitrogen in the Marine Environment. Elsevier Inc., San Diego, CA,
 pp. 631–681.
- Naqvi, S.W.A., Jayakumar, D.A., Narvekar, P. V., Naik, H., Sarma, V.V.S.S., D'Souza, W.,
 Joseph, S., George, M.D., 2000. Increased marine production of N2O due to intensifying anoxiaon the Indian continental shelf. Nature 408, 346–349.
 https://doi.org/10.1038/35042551
- Owens, N.J.P., Burkill, P.H., Mantoura, R.F.C., Woodward, E.M.S., Bellan, I.E., Aiken, J., Howland, R.J.M., Llewellyn, C.A., 1993. Size-fractionated primary production and nitrogen assimilation in the northwestern Indian Ocean. Deep Sea Res. Part II Top. Stud. Oceanogr. 40, 697–709. https://doi.org/http://dx.doi.org/10.1016/0967-0645(93)90053-P
 - Parsons, T.R., Maita, Y., Lalli, C.M., 1984. A manual of chemical and biological methods for seawater analysis. Pergamon, Oxford.
 - Partensky, F., Hess, W.R., Vaulot, D., 1999. Prochlorococcus, a marine photosynthetic prokaryote of global significance. Microbiol. Mol. Biol. Rev. 63, 106–127.
- Prakash, S., Ramesh, R., Sheshshayee, M.S., Mohan, R., Sudhakar, M., 2015. Nitrogen uptake rates and f-ratios in the Equatorial and Southern Indian Ocean. Curr. Sci. 108, 239–245.
 - Price, N.M., Harrison, P.J., 1987. A comparison of methods for the measurement of dissolved urea concentrations in seawater. Mar. Biol. 94, 307–317.
 - Ridal, J.J., Moore, R.M., 1990. A re-examination of the measurement of dissolved organic phosphorus in seawater. Mar. Chem. 29, 19–31.
- Rocap, G., Larimer, F.W., Lamerdin, J., Malfatti, S., Chain, P., Ahlgren, N.A., Arellano, A.,
 Coleman, M., Hauser, L., Hess, W.R., Johnson, Z.I., Land, M., Lindell, D., Post, A.F.,
 Regala, W., Shah, M., Shaw, S.L., Steglich, C., Sullivan, M.B., Ting, C.S., Tolonen, A.,
 Webb, E.A., Zinser, E.R., Chisholm, S.W., 2003. Genome divergence in two
 Prochlorococcus ecotypes reflects oceanic niche differentiation. Nature 424, 1042–1047.
- Roxy, M.K., Modi, A., Murtugudde, R., Valsala, V., Panickal, S., Kumar, S.P., Ravichandran,
 M., Vichi, M., Lévy, M., 2016. A reduction in marine primary productivity driven by rapid
 warming over the tropical Indian Ocean. Geophys. Res. Lett. 43, 826–833.
- 751 https://doi.org/10.1002/2015GL066979

734

735

736

739

740

741

742

Saji, N.H., Goswami, B.N., Vinayachandran, P.N., Yamagata, T., 1999. A dipole mode in the tropical Indian Ocean. Nature 401, 360–363.

- Schlüter, L., Henriksen, P., Nielsen, T.G., Jakobsen, H.H., 2011. Phytoplankton composition and
 biomass across the southern Indian Ocean. Deep Sea Res. Part I Oceanogr. Res. Pap. 58,
 546–556. https://doi.org/http://dx.doi.org/10.1016/j.dsr.2011.02.007
- Schott, F.A., McCreary Jr., J.P., 2001. The monsoon circulation of the Indian Ocean. Prog. Oceanogr. 51, 1–123.
- Sengupta, D., Bharath Raj, G.N., Shenoi, S.S.C., 2006. Surface freshwater from Bay of Bengal
 runoff and Indonesian Throughflow in the tropical Indian Ocean. Geophys. Res. Lett. 33,
 L22609. https://doi.org/10.1029/2006GL027573
- Sherman, E., Moore, J.K., Primeau, F., Tanouye, D., 2016. Temperature influence on
 phytoplankton community growth rates. Global Biogeochem. Cycles 30, 550–559.
 https://doi.org/10.1002/2015GB005272

- Sieracki, M.E., Viles, C.L., Webb, K.L., 1989. Algorithm to estimate cell biovolume using image analyzed microscopy. Cytometry 10, 551–557.
- Singh, A., Baer, S.E., Riebesell, U., Martiny, A.C., Lomas, M.W., 2015. C: N: P stoichiometry
 at the Bermuda Atlantic Time-series Study station in the North Atlantic Ocean.
 Biogeosciences 12. https://doi.org/10.5194/bg-12-6389-2015
- Sorokin, Y.I., Koplyov, A.I., Mamaeva, N. V, 1985. Abundance and dynamics of microplankton in the central tropical Indian Ocean. Mar. Ecol. Prog. Ser. 24, 27–41.
 - Thi Dieu Vu, H., Sohrin, Y., 2013. Diverse stoichiometry of dissolved trace metals in the Indian Ocean. Sci. Rep. 3, 1745. https://doi.org/10.1038/srep01745
- Thomalla, S.J., Waldron, H.N., Lucas, M.I., Read, J.F., Ansorge, I.J., Pakhomov, E., 2011.
 Phytoplankton distribution and nitrogen dynamics in the southwest indian subtropical gyre and Southern Ocean waters. Ocean Sci. 7, 113–127. https://doi.org/10.5194/os-7-113-2011
- Waite, A.M., Thompson, P.A., Pesant, S., Feng, M., Beckley, L.E., Domingues, C.M., Gaughan,
 D., Hanson, C.E., Holl, C.M., Koslow, T., Meuleners, M., Montoya, J.P., Moore, T.,
 Muhling, B.A., Paterson, H., Rennie, S., Strzelecki, J., Twomey, L., 2007. The Leeuwin
 Current and its eddies: An introductory overview. Deep Sea Res. Part II Top. Stud.
 Oceanogr. 54, 789–796. https://doi.org/10.1016/J.DSR2.2006.12.008
- Ward, B.B., Devol, A.H., Rich, J.J., Chang, B.X., Bulow, S.E., Naik, H., Pratihary, A.,
 Jayakumar, A., 2009. Denitrification as the dominant nitrogen loss process in the Arabian
 Sea. Nature 461, 78–81.
- https://doi.org/http://www.nature.com/nature/journal/v461/n7260/suppinfo/nature08276_S1. html
- Weller, R.A., Plueddemann, A.J., 1996. Observations of the vertical structure of the oceanic
 boundary layer. J. Geophys. Res. Ocean. 101, 8789–8806.
 https://doi.org/10.1029/96JC00206
- Wiggert, J.D., Murtugudde, R.G., Christian, J.R., 2006. Annual ecosystem variability in the
 tropical Indian Ocean: Results of a coupled bio-physical ocean general circulation model.
 Deep Sea Res. Part II Top. Stud. Oceanogr. 53, 644–676.
 https://doi.org/http://dx.doi.org/10.1016/j.dsr2.2006.01.027
- Williams, P.J. le B., Quay, P.D., Westberry, T.K., Behrenfeld, M.J., 2013. The oligotrophic
 ocean is autotrophic. Ann. Rev. Mar. Sci. 5, 535–549. https://doi.org/doi:10.1146/annurev-marine-121211-172335
- Zubkov, M. V, Fuchs, B.M., Tarran, G.A., Burkill, P.H., Amann, R., 2003. High rate of uptake
 of organic nitrogen compounds by Prochlorococcus cyanobacteria as a key to their
 dominance in oligotrophic oceanic waters. Appl. Environ. Microbiol. 69, 1299–1304.

Tables & Figures Table 1. Urea and dissolved organic phosphorus (DOP) concentrations, chlorophyll a (chl a) and cell counts for select stations, all at 20 m depth. BD for below detection (0.01 μ mol N L⁻¹).

Samples not taken or where there was a problem with the analysis are indicated as NS.

							x10 ³ cells ml ⁻¹		
					-	hetero-			small
							Prochloro-	Svnecho-	
Stn	Lat.	Long.	Urea	DOP	chl a	bacteria	coccus	coccus	(<20 µm)
	°N	°E	μmol L ⁻¹	μmol L ⁻¹	mg m ⁻³				. ,
84	-28.31	95.00	NS	NS	0.033	77	53	0.66	0.26
87	-26.52	95.00	BD	0.252	0.032	85	58	0.49	0.17
90	-24.73	95.00	0.020	0.278	0.034	85	63	0.51	0.27
91	-24.14	95.00	NS	NS	0.054	93	54	0.38	0.20
94	-22.45	95.00	BD	0.262	NS	94	58	0.38	0.18
97	-20.76	95.00	0.026	NS	0.062	174	83	0.59	0.22
100	-19.08	95.00	NS	NS	NS	133	99	0.39	0.25
103	-17.40	95.00	BD	0.393	0.045	130	103	0.52	0.37
107	-15.17	95.00	0.049	0.282	0.052	197	134	0.71	0.37
110	-13.57	95.00	0.085	0.356	0.070	175	145	1.28	0.34
114	-11.42	95.00	BD	0.320	0.087	210	185	0.74	0.45
116	-10.35	95.00	0.037	0.344	0.092	250	211	0.82	0.62
120	-8.22	95.00	0.014	0.325	0.085	217	193	1.10	0.35
123	-6.60	95.00	BD	0.346	0.111	219	212	1.68	0.31
127	-4.53	94.87	0.069	0.343	0.098	198	171	2.49	0.51
130	-3.13	94.43	0.067	0.356	0.108	163	164	3.34	0.42
133	-2.20	94.13	0.073	0.303	0.123	193	171	7.18	0.43
138	-0.63	93.65	NS	0.318	NS	243	196	8.32	0.44
142	0.55	93.02	0.085	0.291	0.198	228	187	9.74	0.43
145	1.45	92.30	0.067	0.308	0.138	199	169	9.96	0.30
149	3.00	91.76	0.061	0.300	0.147	257	167	6.55	0.19
154	5.02	90.47	0.067	0.371	0.124	253	181	4.44	0.39
158	6.50	89.34	0.097	NS	0.136	245	166	6.45	0.32
162	7.98	88.20	0.049	0.296	NS	258	177	5.42	0.51
166	9.46	87.07	0.091	0.308	0.096	230	173	3.87	0.31
181	10.77	87.34	0.061	0.314	0.096	230	134	2.51	0.27
185	12.66	88.46	0.115	0.264	0.099	185	110	1.24	0.23
189	14.55	89.59	0.145	0.256	0.082	169	100	3.58	0.16
194	17.00	89.85	0.175	0.309	0.129	215	126	1.76	0.20

809	Figure Legends
810	Figure 1. Cruise track for GO-SHIP cruise IO9N in 2016. Cruise stations, where CTD casts
811	were performed, are black circles; white circles are stations where uptake experiments were
812	performed. The cruise traveled from south to north, starting in Perth, Australia on March 21,
813	2016, ending in Phuket, Thailand, on April 28, 2016. The dashed lines separate the regions
814	identified as probable biogeochemical zones, as defined in the text: Indian Southern Subtropical
815	Gyre (ISSG), Central Indian Ocean (CIO), and InterMonsoon Gyre (IMG).
816	
817	Figure 2. Temperature (gray scale shading) and salinity (contour lines) data along the
818	transect. Data derived from the CTD downcast, and values were averaged into 1 m bins before
819	plotting. Dashed lines represent divisions between biogeochemical zones, as described in the
820	text and shown in Figure 1.
821	
822	Figure 3. Description of important physical and chemical depth horizons and nutrient
823	fluxes along the transect. A) Mixed layer (filled diamonds) and nutricline (open diamonds)
824	depths at each station. Mixed layer depth was determined as the first depth at which sigma-t was
825	0.03 units above the value at the surface (0 m) and nutricline depth was determined as the first
826	depth where nitrate measurements exceeded 0.05 μM . B) Nitrate (filled circles) and phosphate
827	(gray circles) flux rates across the nutricline at each station. C) The ratio of nitrate to phosphate
828	fluxes at each station. Horizontal dashed lines represent divisions between biogeochemical
829	zones, as described in the text and shown in Figure 1.
830	
831	Figure 4. Nitrate (panel A) and phosphate (panel B) concentrations in the surface 200 m
832	along the transect. Nitrate: phosphate ratios (N:P; panel C) for all locations and depths where
833	there was measurable nitrate to derive a meaningful ratio. Black dots represent sampling
834	locations and depths. Dashed lines represent divisions between biogeochemical zones, as
835	described in the text and shown in Figure 1.
836	
837	Figure 5. Microbial biomass estimates ($\mu g \ C \ L^{-1}$) along the transect. Samples for
838	phytoplankton and heterotrophic bacteria were collected at 20 m depth and abundance converted
839	to biomass based on the flow cytometric forward scatter to carbon relationship empirically

determined by Casey et al. (2013) for autotrophs, and a value of 12 fg C cell⁻¹ for heterotrophic 840 841 bacteria (Fukuda et al., 1998). Large phytoplankton (>20 µm) were enumerated by FlowCam 842 and converted to biomass based on biovolume relationships to carbon (Menden-Deuer and 843 Lessard, 2000; Sieracki et al., 1989). Horizontal dashed lines represent divisions between 844 biogeochemical zones, as described in the text and shown in Figure 1. 845 846 Figure 6. Near surface (20m) carbon and nitrogen uptake rates measured along the **transect.** A) Absolute uptake rates of nitrate (NO₃⁻; filled squares), ammonium (NH₄⁺; open 847 848 circles), and urea (gray triangles); B) f-ratio (filled diamonds); C) absolute uptake rates of carbon 849 as bicarbonate (primary production); D) ratio of carbon:nitrate (C:NO₃) uptake rates. Horizontal 850 dashed lines represent divisions between biogeochemical zones, as described in the text and 851 shown in Figure 1. 852 853 Figure 7. Estimated autotrophic growth rates along the transect. Growth rates were 854 calculated from absolute C uptake rates, scaled to biomass and available PAR, as described in 855 section 2.5 of the methods. Horizontal dashed lines represent divisions between biogeochemical 856 zones, as described in the text and shown in Figure 1. 857 858 Figure 8. Relationships between phytoplankton biomass, primary production and depth. 859 A) Total phytoplankton biomass (the sum of biomass estimates for *Prochlorococcus*, 860 Synechococcus, small eukaryotes, and large phytoplankton) correlated with absolute carbon 861 uptake rates. Black lines are the best-fit Model I regression and dashed lines are the 95% 862 confidence intervals. B) Total phytoplankton biomass as a function of mixed layer depth (filled 863 diamonds) and nutricline depth (open diamonds) as defined in Figure 3. Black lines are the best-864 fit polynomial inverse first order correlations and dashed lines are the 95% confidence intervals.

866 Figure 1.

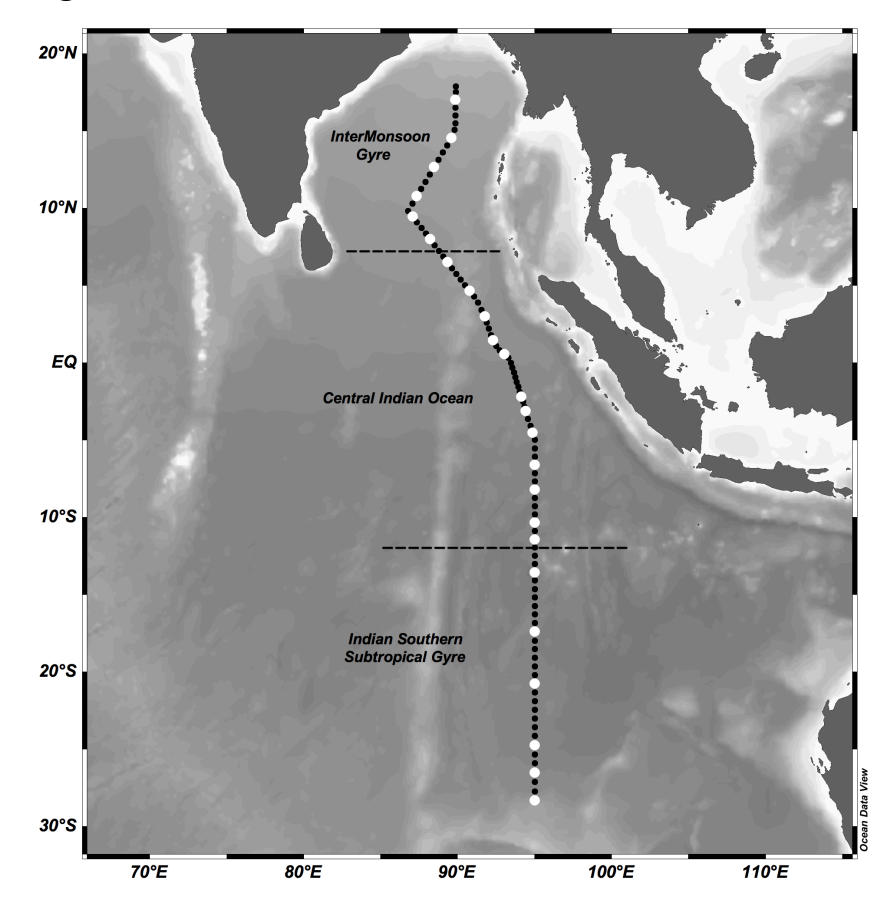


Figure 2.

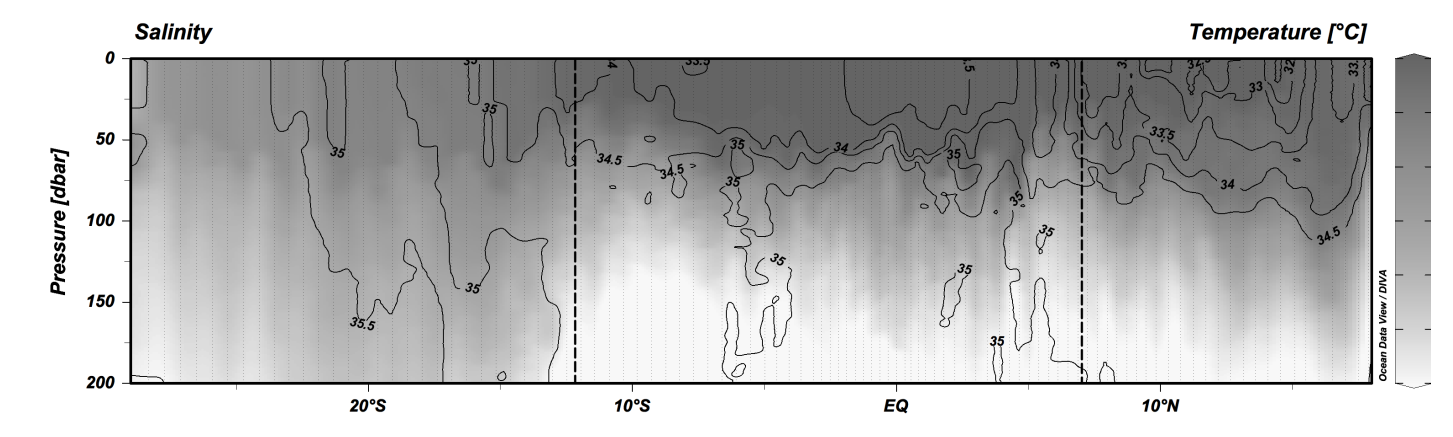


Figure 3 873

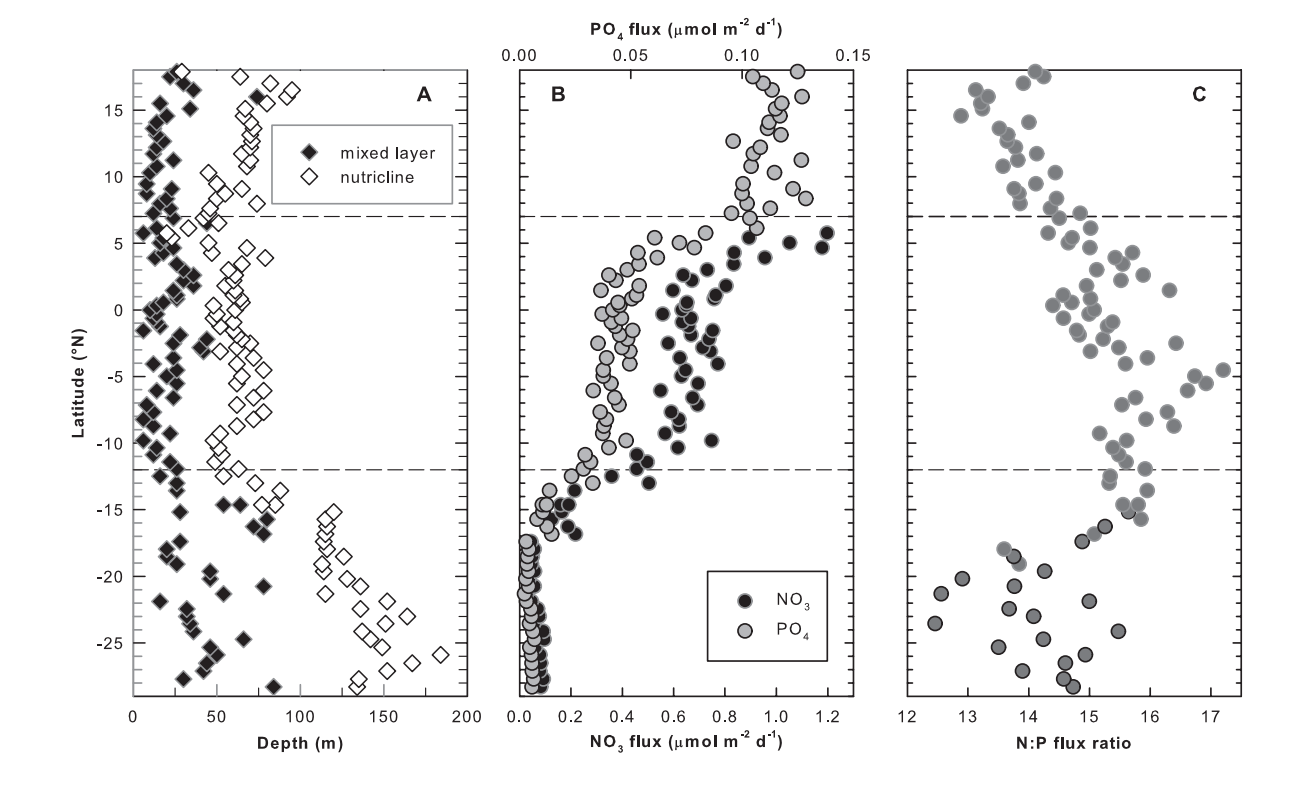


Figure 4.

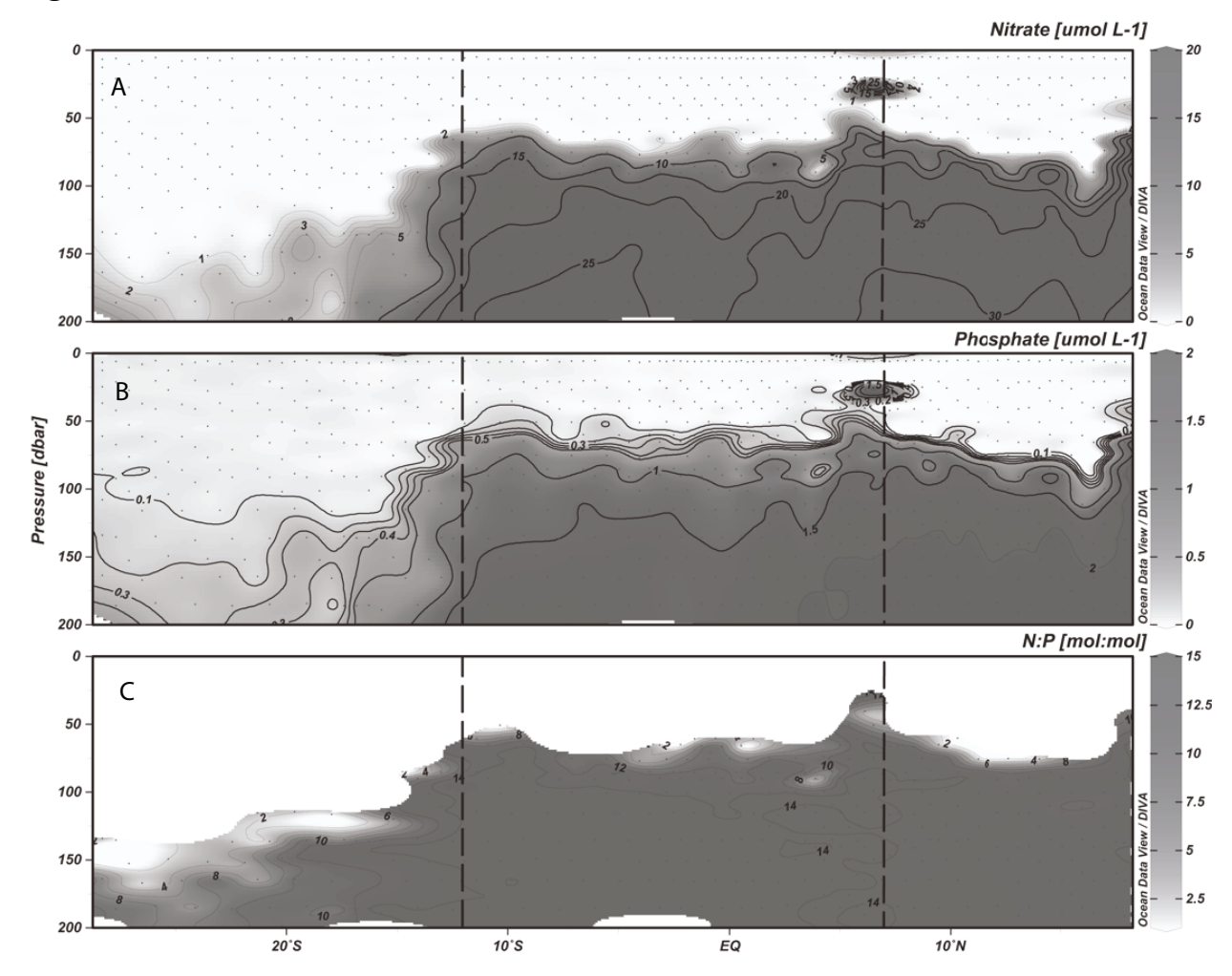
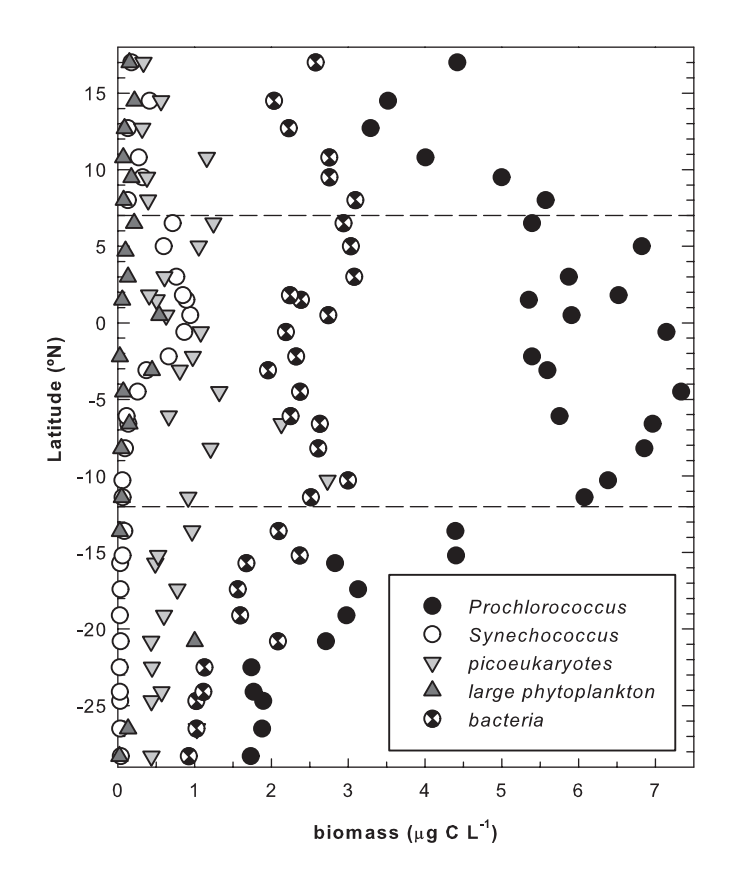


Figure 5 880



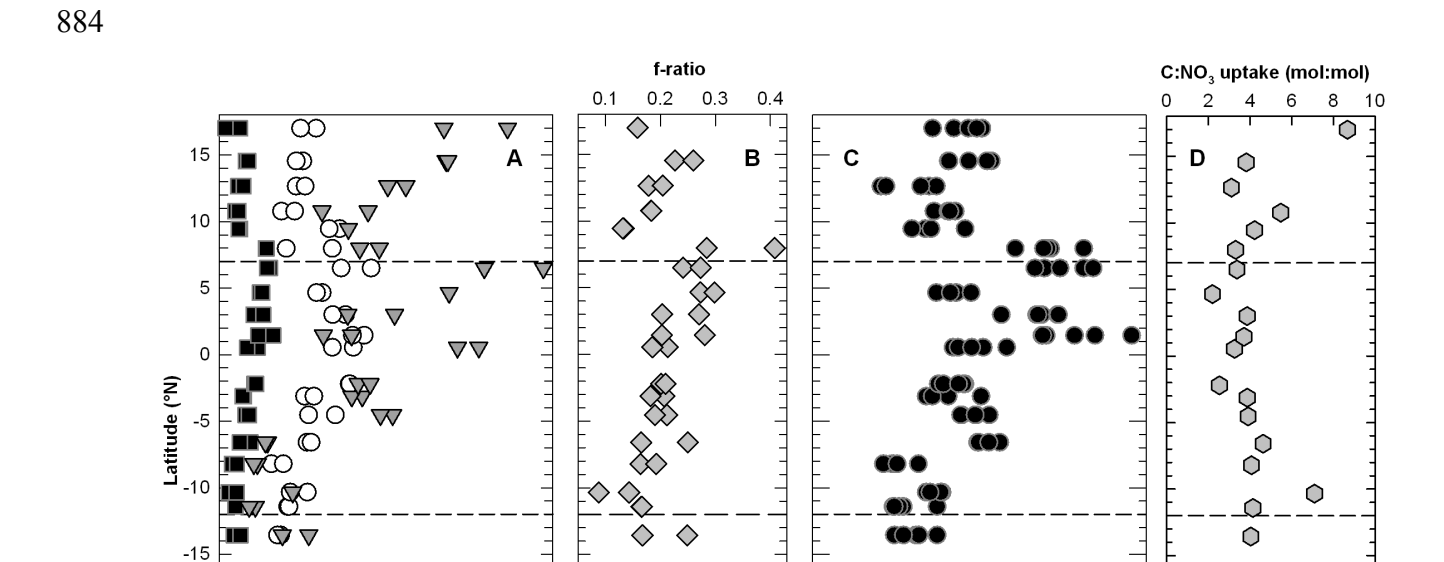
883 **Figure 6.**

-20

-25

885

Absolute uptake (nmol N L⁻¹ h⁻¹)



0

0

Primary production (nmol C L^{-1} h^{-1})

Figure 7 887

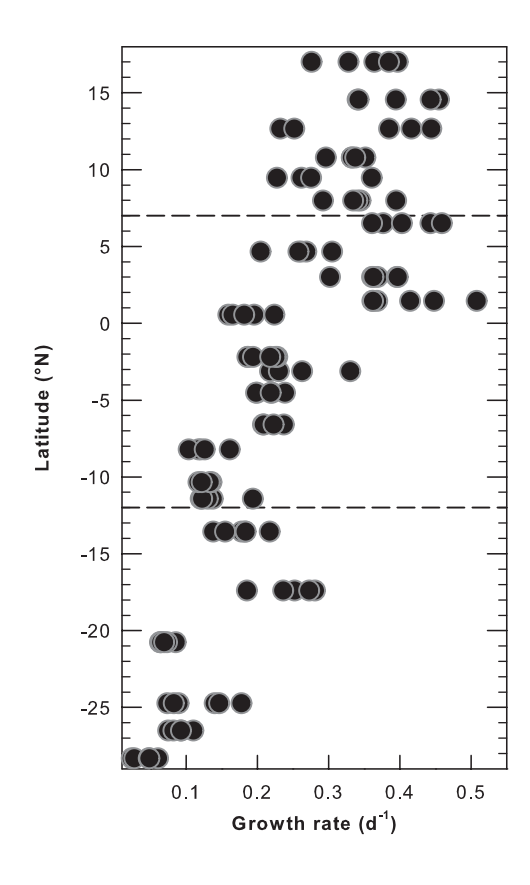
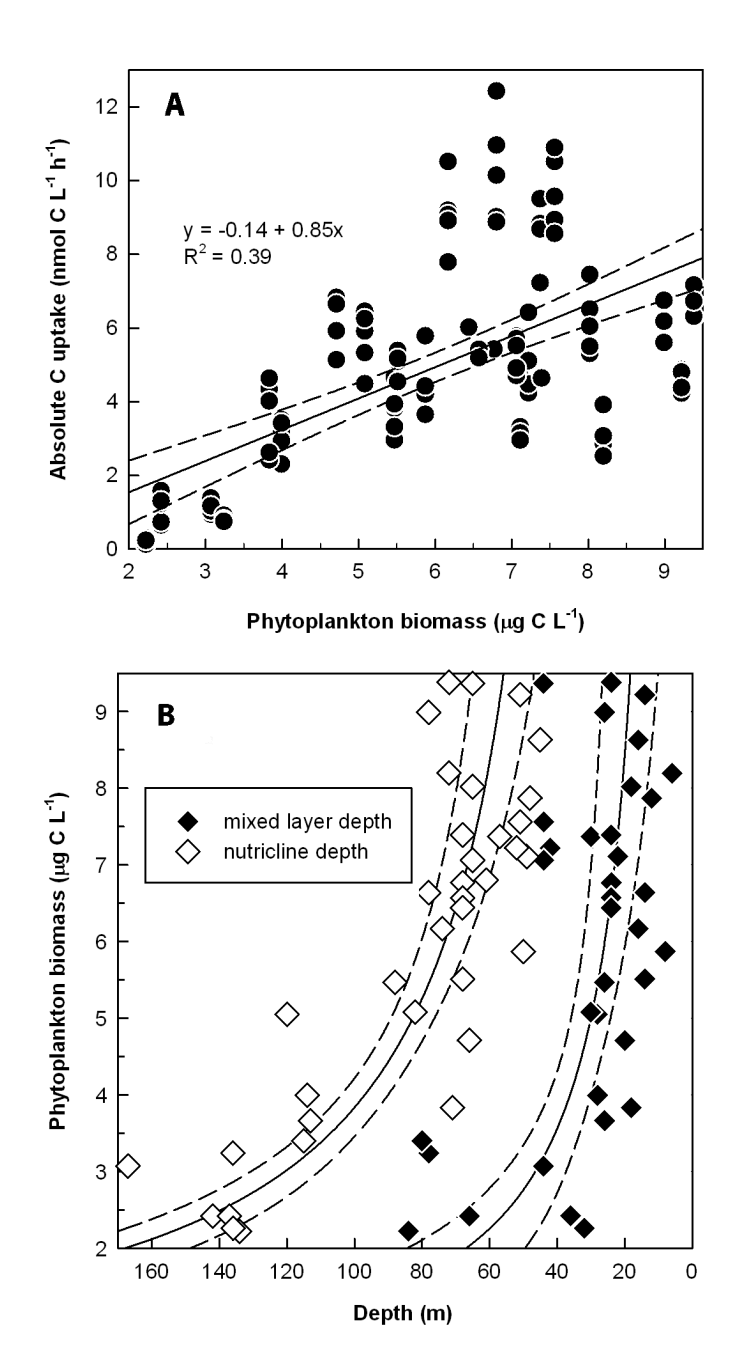


Figure 8 890



Supplementary Materials

Figure S1. Temperature trace inside incubation bottles during deckboard incubations. Temperatures were recorded by a HOBO temperature logger (Onset Computer Corp. Falmouth MA) at one minute intervals. The logger was placed inside a 2L HDPE bottle filled with ambient seawater and included in the on-deck incubation system. Each line represents a distinct station incubation, as indicated by the legend as station number (latitude). Ambient temperature is the left-most point of each line.

